journal of the mechanical behavior of biomedical materials 126 (2022) 105021

Contents lists available at ScienceDirect

Journal of the Mechanical Behavior of Biomedical Materials

journal homepage: www.elsevier.com/locate/jmbbm

Passive biaxial mechanical behavior of newborn mouse aorta with and without elastin

Jungsil Kim [a], Austin J. Cocciolone [b], Marius C. Staiculescu [a], Robert P. Mecham [c], Jessica E. Wagenseil [a,*]

[a] Department of Mechanical Engineering and Materials Science, Washington University, St. Louis, MO, USA
[b] Department of Biomedical Engineering, Washington University, St. Louis, MO, USA
[c] Department of Cell Biology and Physiology, Washington University, St. Louis, MO, USA

ARTICLE INFO

Keywords:
Elastin
Aorta
Biomechanics
Constitutive modeling
Maturation

ABSTRACT

Aortic wall material properties are needed for computational models and for comparisons across developmental and disease states. There has been abundant work in comparing aortic material properties across disease states, but limited work across developmental states. We performed passive biaxial mechanical testing on newborn mouse aorta with ($Eln^{+/+}$) and without ($Eln^{-/-}$) elastin. Elastin provides elasticity to the aortic wall and is necessary for survival beyond birth in the mouse. Mechanically functional elastin is challenging to create in vitro and so $Eln^{-/-}$ aorta can be a comparison for tissue engineered arteries with limited elastin amounts. We found that a traditional arterial strain energy function provided reasonable fits to newborn mouse aorta and generally predicted lower material constants in $Eln^{-/-}$ compared to $Eln^{+/+}$ aorta. At physiologic pressures, the circumferential stresses and moduli trended lower in $Eln^{-/-}$ compared to $Eln^{+/+}$ aorta. Increased blood pressure in $Eln^{-/-}$ mice helps to alleviate the differences in stresses and moduli. Increased blood pressure also serves to partially offload stresses in the isotropic compared to the anisotropic component of the wall. The baseline material parameters can be used in computational models of growth and remodeling to improve understanding of developmental mechanobiology and tissue engineering strategies.

1. Introduction

Passive biaxial mechanical behavior of adult mouse aorta has been well-characterized and has provided insight into how mechanical changes in the aortic wall may be linked to disease progression (Bellini et al., 2017). However, adult mouse aorta represents an already remodeled or diseased state and does not provide information on how the aorta progressed to the current state. Growth and remodeling models have been used to understand how mechanical forces during development and maturation contribute to mechanical behavior of the adult aorta (Wagenseil, 2011), but there is limited experimental data to inform starting material parameters for embryonic or newborn aorta (Murtada et al., 2021; Cheng et al., 2013).

We performed passive biaxial mechanical testing on newborn (<24 h old) mouse aorta to quantify mechanical behavior at this young age. We fitted a constitutive model based on a fiber-reinforced composite that has been used extensively for adult aorta (Holzapfel et al., 2000). We previously used a similar model to calculate elastin and collagen contributions in maturing mouse aorta from 3 to 60 days of age (soon after birth to adulthood) and predict how these contributions change with postnatal maturation and elastin haploinsufficiency ($Eln^{+/-}$) (Cheng et al., 2013). Elastin is the core component of elastic fibers that provide reversible distensibility to the large, conduit arteries. Collagen provides strength and limits over-distension of the arterial wall at high pressures.

We compared passive biaxial mechanical behavior of control (wild-type) aorta to aorta from mice that do not express elastin ($Eln^{-/-}$). $Eln^{-/-}$ mice die soon after birth from severe elastic fiber defects (Li et al., 1998). We previously showed that the absence of elastin leads to increased stiffness (Wagenseil et al., 2009) and energy dissipation (Kim et al., 2017) in the newborn mouse aorta, confirming the role of elastic fibers in providing elasticity to the aortic wall. Our previous study did not include biaxial mechanical data or fitting of constitutive models to fully characterize changes in aortic material behavior.

Our current results provide biaxial material properties for newborn

* Corresponding author. Department of Mechanical Engineering and Materials Science, Washington University, One Brookings Dr., MSC-1185-208-125, St. Louis, MO, 63130, USA.
E-mail address: jessica.wagenseil@wustl.edu (J.E. Wagenseil).

https://doi.org/10.1016/j.jmbbm.2021.105021
Received 10 September 2021; Received in revised form 16 November 2021; Accepted 28 November 2021
Available online 29 November 2021

wild-type mouse aorta that are applicable for growth and remodeling studies and for $Eln^{-/-}$ mouse aorta that are relevant to elastic fiber disease (Merla et al., 2012) and tissue engineered arteries (Patel et al., 2006) with absent or reduced amounts of functional elastic fibers. Our constitutive model also provides insight into the contributions of elastic fibers to biaxial mechanics in the maturing mouse aorta.

2. Methods

2.1. Animals

$Eln^{+/-}$ mice (Li et al., 1998) were bred to produce $Eln^{-/-}$ and $Eln^{+/+}$ pups. All pups were sacrificed within 24 h after birth by thoracotomy under 2.5% isoflurane or CO_2 inhalation. Ascending aortic (AA) segments from the root to the brachiocephalic artery were used for all studies. Sex of the animals was not determined. All animal protocols were approved by the Institutional Animal Care and Use Committee at Washington University.

2.2. Wall structure

AAs were frozen in optimal cutting temperature media, sectioned on a cryostat, and fluorescently stained to visualize wall structure. Elastin was stained with Alexa Fluor 633 Hydrazide (0.6 μM, Life Technologies) (Shen et al., 2012; Clifford et al., 2011). Collagen was stained with CNA35 (kindly provided by Magnus Hook, Texas A&M) labeled with Oregon Green 488 (Life Technologies) (5 μM) (Krahn et al., 2006). Cell nuclei were stained with Hoechst 34580 (5 μM, Life Technologies). Images were taken on a Zeiss 710 confocal microscope at 40× magnification. Three – four AAs from each genotype were examined.

2.3. Passive mechanical testing

AAs were stored in physiologic saline solution at 4 °C for up to two days before testing (Amin et al., 2011). The AA was mounted on custom stainless steel cannulae that have machined grooves to hold 7-0 silk suture ties in a 37 °C Myograph 110P (Danish Myotechnology) bath filled with physiologic saline solution (Amin et al., 2012). The AA was stretched axially to 1.05 times the unloaded length between sutures ties, and preconditioned circumferentially by pressurizing for three cycles from 0 to 60 mmHg. The pressure range was chosen based on previous systolic blood pressure measurements in newborn $Eln^{+/+}$ and $Eln^{-/-}$ mice (Wagenseil et al., 2009). The AA was preconditioned axially by stretching from approximately 1.05–1.25 the unloaded length at 0 mmHg. The axial stretch values varied slightly for each AA to avoid overstretch and irreversible damage.

After preconditioning, the AA was subjected to three constant length inflation cycles from 0 to 60 mmHg near 1.05, 1.15, and 1.25 times the unloaded length and three constant pressure axial stretch cycles near 1.05–1.25 times the unloaded length at 12, 24, and 36 mmHg. For the inflation cycles, the AA was pressurized in 5 mmHg step increments, holding for 12 s at each step. For the axial stretch cycles, the AA was stretched by manually turning a micrometer attached to one end of the AA at a rate of approximately 20 μm/s. Three of each inflation or axial stretch cycles were performed while recording outer diameter, lumen pressure, and longitudinal force at 2 Hz. Axial stretch with respect to the unloaded configuration was calculated based on the distance traveled by the artery mounting rod. Only AAs that underwent all six mechanical testing protocols were included in the data analysis. A total of seven $Eln^{+/+}$ and six $Eln^{-/-}$ AAs were included in the analyses. The pressure-outer diameter data for one inflation cycle at 1.05 axial stretch have been previously published (Kim et al., 2017). Cross-sectional rings were cut after testing and imaged to determine the AA unloaded thickness.

2.4. Data analyses

The unloaded thickness (T) was determined by averaging four linear measurements across the wall in three cross-sectional rings for each AA. The unloaded outer diameter (D_o) was determined from the minimum diameter at 0 mmHg from the mechanical testing data. The unloaded inner diameter is $D_i = D_o - 2T$. The unloaded diameter and thickness values have been previously published (Kim et al., 2017). Unless there was a problem with video tracking of the AA diameter, the third recorded loading cycle was used for all analyses. The loaded inner diameter (d_i) was calculated from the unloaded dimensions assuming incompressibility (Faury et al., 1999). Although a thin-walled approximation is not appropriate for newborn mouse aorta because the radius to thickness ratio is approximately three, radial variations in stress and strain were ignored by using the average stress and strain values (Ferruzzi et al., 2013). Since the AA loading and unloading behavior is repeatable at the constant strain rates after preconditioning, we applied the concept of pseudo-elasticity and analyzed only the loading curves (Fung, 1993).

Assuming the aorta acts as an incompressible cylinder with no shear, the mean arterial wall stresses in the circumferential ($\sigma_{\theta\theta}$) and axial (σ_{zz}) direction can be calculated from:

$$\sigma_{\theta\theta} = \frac{Pr_i}{r_o - r_i} \tag{1}$$

$$\sigma_{zz} = \frac{f + Pr_i^2}{\pi\left(r_o^2 - r_i^2\right)} \tag{2}$$

where P is the internal pressure, f is the measured axial force, r_i is the inner radius and r_o is the outer radius of the inflated aorta.

2.5. Constitutive modeling

For an axisymmetric cylinder subjected to non-linear, large elastic deformation in the absence of shear, the inflation and extension of the aorta can be described by the deformation gradient (**F**) and the right Cauchy-Green (**C**) strain tensor:

$$[\boldsymbol{F}] = diag[\lambda_\theta, \lambda_z, \lambda_r] \tag{3}$$

$$[\boldsymbol{C}] = diag\left[\lambda_\theta^2, \lambda_z^2, \lambda_r^2\right] \tag{4}$$

where λ_i are the stretch ratios in each direction (θ = circumferential z = axial, and r = radial) defined by:

$$\lambda_\theta = \frac{r}{R},\ \lambda_z = \frac{l}{L},\ \lambda_r = \frac{\partial r}{\partial R} \tag{5}$$

and r and R are the radii of the deformed and undeformed configurations, and l and L are the axial lengths in the deformed and undeformed configurations.

For an incompressible cylinder, the relevant principle stresses can be calculated as:

$$\sigma_{ii} = 2F_{ii}^2\frac{\partial W}{\partial C_{ii}} - p,\ (\text{not summed}) \tag{6}$$

where $i = \theta$, r, or z, and p is the Lagrange multiplier. Inflation and extension in the absence of shear requires $\sigma_{r\theta} = \sigma_{rz} = \sigma_{\theta z} = 0$.

The passive strain energy function (W) for the aortic wall is represented as a fiber-reinforced composite with an isotropic term (I) and an anisotropic term (A) (Holzapfel et al., 2000):

$$W = W^I + W^A \tag{7}$$

The isotropic term is a neo-Hookean solid:

$$W^I = \frac{c_1}{2}(I_1 - 3) \tag{8}$$

where c_1 is a material parameter, and the first invariant is $I_1 = trC = \lambda_\theta^2 + \lambda_z^2 + \lambda_r^2$. The anisotropic term is two symmetrically oriented fiber-families with exponential behavior:

$$W^A = \sum_{k=1}^{2} \frac{c_2}{2c_3}\left(e^{c_3\left(I_4^k-1\right)^2} - 1\right) \tag{9}$$

where c_2 and c_3 are material parameters and I_4 is the fourth invariant for the kth fiber-family as defined by:

$$I_4^k = \lambda_\theta^2 cos^2\left(\alpha^k\right) + \lambda_z^2 sin^2\left(\alpha^k\right) \tag{10}$$

where $\pm\alpha$ represents the angle of the fiber families in the unloaded configuration with respect to the circumferential direction. The linearized elastic moduli in the circumferential (ζ_θ) and axial (ζ_z) directions were calculated by (Baek et al., 2007):

$$\zeta_\theta = 4\lambda_\theta^2 \frac{\partial W}{\partial C_{\theta\theta}} + 4\lambda_\theta^4 \frac{\partial^2 W}{\partial C_{\theta\theta}^2} \tag{11}$$

$$\zeta_z = 4\lambda_z^2 \frac{\partial W}{\partial C_{zz}} + 4\lambda_z^4 \frac{\partial^2 W}{\partial C_{zz}^2} \tag{12}$$

2.6. Parameter fitting

The material parameters ($c_1 - c_3$) and unloaded fiber family angle (α) were determined by constrained nonlinear regression to minimize the error between the experimental and predicted circumferential and axial stress values for every data point, i, using the *fmincon* function in Matlab (Mathworks). The error is defined as:

$$\text{error} = \sqrt{\frac{\sum\left(\sigma_{\theta\theta,\text{exp}}(i) - \sigma_{\theta\theta,pred}(i)\right)^2}{\sum\left(\sigma_{\theta\theta,\text{exp}}(i)\right)^2}} + \sqrt{\frac{\sum\left(\sigma_{zz,\text{exp}}(i) - \sigma_{zz,pred}(i)\right)^2}{\sum\left(\sigma_{zz,\text{exp}}(i)\right)^2}} \tag{13}$$

The material parameters were constrained to the positive domain, and α was only allowed to vary between 0° and 90° with 0° aligning with the circumferential axis. Parameter fitting was performed on data for each individual aorta. Multiple initial parameter estimates were randomly generated to ensure a global minimum was found. Preliminary results showed that some minimum stress contribution was needed for the isotropic term to prevent it having zero contribution in both *Eln*$^{-/-}$ and *Eln*$^{+/+}$ AA. Hence we implemented a constraint that the minimum stress contribution from the isotropic term was at least 10% of the total circumferential stress over the entire loading protocol, as we have done previously in fitting constitutive equations to young mouse aorta (Cheng et al., 2013). Specifically, the constraint:

$$\sigma_{\theta\theta}^I / \sigma_{\theta\theta} > 10\% \tag{14}$$

was implemented. To enforce the constraint in Eqn. (14), a penalty function was included in the final minimization function:

$$\text{min\_error} = \text{error} + \sum(\text{penalty}(i))^2 \tag{15}$$

where *penalty*(i) is a penalty function applied to each data point, i, to enforce the minimum circumferential stress contribution of the isotropic term. The penalty function is:

$$\text{penalty}(i) = 0.1 - \frac{\sigma_{\theta\theta}^I}{\sigma_{\theta\theta}} \text{ if } \frac{\sigma_{\theta\theta}^I}{\sigma_{\theta\theta}} < 0.1 \tag{16}$$

2.7. Statistical analyses

All values are presented as individual data points (when possible) with mean and standard deviation. Results were compared with an unpaired, two-tailed t-test with Welch's correction for unequal standard deviations or with a one-way ANOVA followed by Tukey's multiple comparison test using GraphPad Prism software. $P < 0.05$ was considered significant, while $P < 0.1$ was considered a trend.

3. Results

3.1. Wall structure of newborn mouse AA

Representative images of the elastin, collagen, and cell nuclei in the AA wall are shown in Fig. 1. In *Eln*$^{+/+}$ AA, cell nuclei are organized in layers surrounded by elastin throughout the medial (middle) layer of the wall. Faint collagen signal is detected in the medial layer, with larger collagen amounts in the adventitial (outer) layer of the wall. In *Eln*$^{-/-}$ AA, there are still layers of cell nuclei, but there is no elastin present in the wall. The collagen signal is strong throughout the wall thickness. The increased collagen signal in *Eln*$^{-/-}$ AA may be due to more collagen being available for binding to the CNA35-Oregon Green 488 in the absence of elastin, as collagen amounts measured by a biochemical assay for hydroxyproline are similar between the two genotypes (Kim et al., 2019). The *Eln*$^{-/-}$ AA wall is thicker than *Eln*$^{+/+}$, as confirmed by unloaded dimension measurements (Fig. 2c).

3.2. Passive biaxial mechanical behavior of newborn mouse AA

Images of an *Eln*$^{+/+}$ AA at 1.15 times the unloaded length and inflated to 0 and 60 mmHg are shown in Fig. 2a and b. The average unloaded diameter and thickness values are shown in Fig. 2c. Individual values are provided in Supplemental Table S1. The AA starts out cylindrical at 0 mmHg, but approaches a spherical shape at 60 mmHg, indicating that the cylindrical assumption may not be valid for the entire loading protocol. The length:diameter ratio is approximately 2:1 at 0 mmHg, so end effects may be significant. We developed a preliminary finite element model in Comsol based on Brinkley et al. (Brinkley, 2006) using the average unloaded dimensions, fitted parameters, and different length:diameter ratios for each genotype. For all length:diameter ratios >1, the finite element model predicted diameters and axial forces at the mid-axial region were consistent with the experimental values shown in Fig. 3, indicating that the material parameters fitted using our simplifying assumptions can reproduce the experimental results.

Representative pressure-diameter-force-axial stretch (Fig. 3) and stress-stretch (Fig. 4) data show the expected nonlinear behavior for the mouse AA (Bellini et al., 2017; Cheng et al., 2013). The force consistently decreased with increasing pressure, even at the higher axial stretch values. This behavior is unlike adult mouse arteries where the force increases with increasing pressure at axial stretches above physiologic values (Ferruzzi et al., 2013). In preliminary experiments, increasing the axial stretch caused irreversible damage and plastic deformation of the AA, so conservative values were used for the axial stretch in all experiments and the AA may not have been stretched enough to reach a point of increasing force with pressure. The predicted data from fitting the material parameters in the strain energy function are overlaid with the experimental data in Figs. 3 and 4.

3.3. Fitted material parameters for newborn mouse AA

Overall, the strain energy function showed a reasonable fit to the experimental data (R^2 = 0.64–0.84), with R^2 for *Eln*$^{-/-}$ AAs trending lower than *Eln*$^{+/+}$ AAs ($P = 0.053$, Fig. 5a). Multiple strain energy functions previously used for arterial tissue, including modifications of the current fiber-reinforced composite function with three fiber families (Cheng et al., 2013), four fiber families (Baek et al., 2007), or two to three fiber families with a fiber dispersion function for the symmetrically oriented pair of fiber families (Gasser et al., 2006) and Fung-type functions with seven (Chuong and Fung, 1986) or four parameters (Takamizawa and Hayashi, 1987), were fitted to the experimental data with only small increases in R^2 for either genotype, despite increases in the number of fitted parameters in most cases. For all strain energy

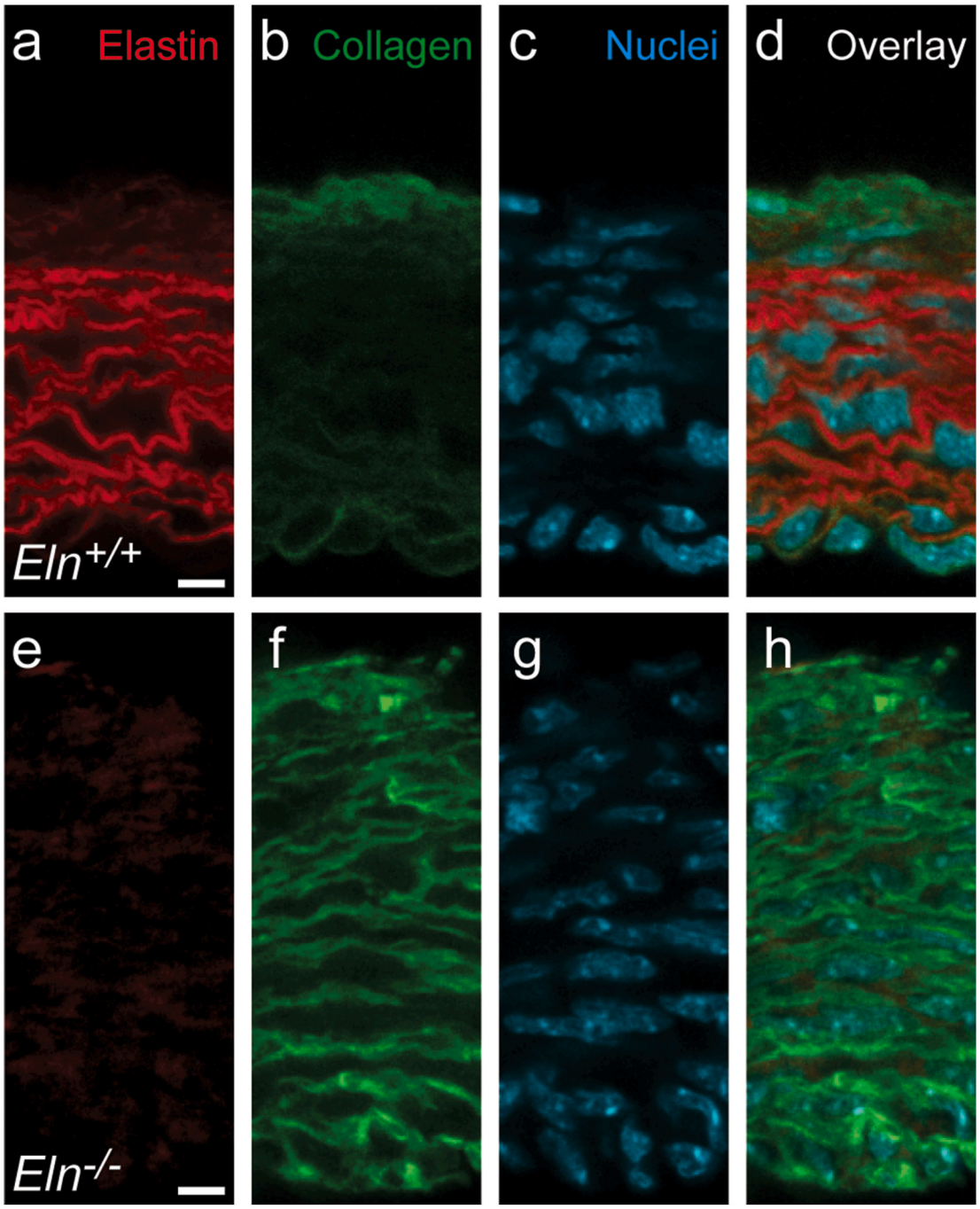

Fig. 1. Aortic wall structure. Cross-sections of newborn $Eln^{+/+}$ (a–d) and $Eln^{-/-}$ (e–h) AA stained for elastin (a,e), collagen (b,f), cell nuclei (c,g), and composite (d, h). Scalebar = 10 μm.

functions, R^2 for $Eln^{-/-}$ AAs trended lower than $Eln^{+/+}$ AAs (Supplemental Table S2 – S8).

The fitted material parameters are shown in Fig. 5. The isotropic constant, c_1, is 37% lower in $Eln^{-/-}$ compared to $Eln^{+/+}$ AA (Fig. 5b). For the anisotropic fibers, the first material constant, c_2, is 52% lower in $Eln^{-/-}$ compared to $Eln^{+/+}$ AA (Fig. 5c), while the second material constant, c_3, is similar between groups (Fig. 5d). The angle, α, of the anisotropic fibers is similar between groups (Fig. 5e). The ratio of c_2/c_3 is a measure of the nonlinearity of the anisotropic fibers and is similar between groups (Fig. 5f). Individual values for the fitted material constants for each aorta for all strain energy functions are provided in Supplemental Table S2 – S8.

3.4. Physiologic mechanical states for newborn mouse AA

It is necessary to compare the mechanical state of the newborn mouse AA in each genotype under physiologically relevant loading conditions. To do this, we chose a standard axial stretch of 1.05, as this was our first common inflation protocol and previous data showed this to be a reasonable approximation for newborn mouse aorta (Kim et al., 2015). We then determined the circumferential stretch ratio from our experimental data at the measured systolic pressure in each genotype. We recently measured the average systolic pressures to be 31 and 41 mmHg in newborn $Eln^{+/+}$ and $Eln^{-/-}$ mice, respectively (Kim et al., 2019). For comparison, we also calculated the $Eln^{-/-}$ AA mechanical states at the $Eln^{+/+}$ blood pressure value of 31 mmHg. The physiologic

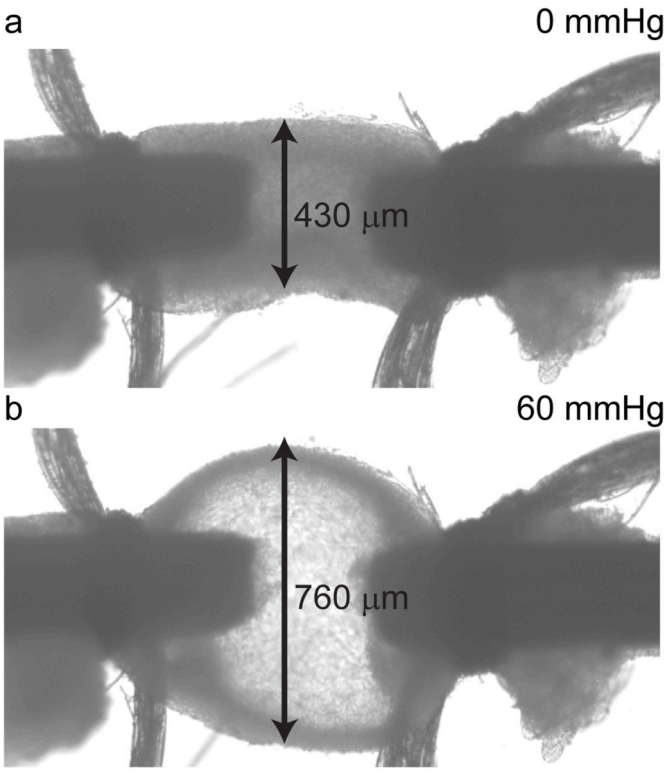

c

Genotype	Unl OD (μm)	Unl thick (μm)
$Eln^{+/+}$	441 ± 29	62 ± 5
$Eln^{-/-}$	377 ± 23	88 ± 4
P value	0.002	< 0.001

Fig. 2. Aortic mechanical testing. $Eln^{+/+}$ AA mounted in the mechanical test system at 1.15 axial stretch and inflated to 0 (a) and 60 (b) mmHg. Outer diameter in the region of maximum dilation is shown. Unloaded outer diameters and thicknesses (mean ± SD) measured from cut rings after mechanical testing are shown in c. N = 6–7/group. P values from two-tailed *t*-test with Welch's correction for unequal standard deviations.

circumferential stretch ratios (Fig. 6a) and linearized axial moduli (Fig. 6f) are not significantly different between genotypes. The circumferential stresses (Fig. 6b) and stored strain energies (Fig. 6d) at physiologic pressures are not different between genotypes, but are significantly reduced in $Eln^{-/-}$ compared to $Eln^{+/+}$ AA at a common pressure of 31 mmHg. The physiologic axial stresses are 42–56% lower (Fig. 6c) and the incremental circumferential moduli are 32–63% lower (Fig. 6e) in $Eln^{-/-}$ compared to $Eln^{+/+}$ AA. In all cases where the physiologic mechanical states are lower in $Eln^{-/-}$ compared to $Eln^{+/+}$ AA, the differences would have been even greater if the $Eln^{-/-}$ mice had comparable blood pressure to $Eln^{+/+}$ mice (e.g. Fig. 6b–e).

We are interested in comparing the relative contributions of the isotropic and anisotropic components to the physiologic stresses to better understand developmental AA mechanics and remodeling due to the lack of elastin. The isotropic contribution to the circumferential and axial stresses ranges from 14 to 42% (Fig. 7a and b). The isotropic stress ratios are not significantly different between genotypes at their physiologic pressures, but are significantly different or trend towards reduced values in $Eln^{-/-}$ compared to $Eln^{+/+}$ AA at a common pressure of 31 mmHg. The anisotropic contribution makes up the rest of the total stresses and is 58–86% in each direction (Fig. 7c and d). The increased physiologic pressure in $Eln^{-/-}$ mice serves to increase the anisotropic stress contribution and decrease the isotropic stress contribution compared to values calculated at $Eln^{+/+}$ physiologic pressure.

4. Discussion

4.1. Elastin and aortic development

Elastin is uniquely designed to provide elasticity to tissues that undergo passive stretch and cyclic loading, including the large arteries, the bladder, and the lungs. In the large arteries, elastin allows the wall to stretch during systole and elastically recoil during diastole, doing work to aid the heart in circulating blood. In the mouse aorta, collagen and elastin deposition begin late in embryonic development and continue through early postnatal maturation, following a similar temporal increase to blood pressure and flow, and suggesting that these extracellular matrix proteins are laid down either in response to or in preparation for increases in hemodynamic forces (Wagenseil and Mecham, 2009). A better understanding of mechanically induced remodeling during aortic development is critical for recreating the process in tissue-engineering and manipulating the process for disease interventions and treatments. A key starting point is quantification of aortic material properties at different developmental stages. While many groups have focused on mechanical characterization of the adult aorta, there is limited experimental data on late embryonic and newborn aorta (Murtada et al., 2021; Cheng et al., 2013). Here, we present biaxial mechanical data on the AA from newborn mice to provide a starting point for predictions of growth and remodeling mechanisms during a critical time of extracellular matrix deposition and hemodynamic alterations.

Newborn $Eln^{-/-}$ mice are a unique resource to investigate aortic growth and remodeling in the presence of perturbations to extracellular matrix amounts and hemodynamic forces. $Eln^{-/-}$ AA has no elastin, increased numbers of smooth muscle cells, and similar collagen amounts to $Eln^{+/+}$ (Wagenseil et al., 2009; Kim et al., 2019). $Eln^{-/-}$ mice die soon after birth due to overproliferation of smooth muscle cells that occlude the aortic lumen (Li et al., 1998). At embryonic day 18, 2–3 days before birth, $Eln^{-/-}$ mice have a longer, thicker aorta with increased stiffness, but do not have high blood pressure or compromised heart function compared to $Eln^{+/+}$ mice (Wagenseil et al., 2010). At birth, $Eln^{-/-}$ mice continue to have a longer, thicker aorta with increased stiffness, and also have high blood pressure and compromised heart function, including reduced ejection fraction and cardiac output, compared to $Eln^{+/+}$ mice (Wagenseil et al., 2009). Although we had previously quantified the morphology, dimensions, and stiffness in $Eln^{-/-}$ aorta, we had not fully investigated the passive biaxial mechanical behavior of the wall and how it may adapt to the absence of elastin and the resulting alterations in hemodynamic forces.

4.2. Alterations to aortic mechanical behavior in the absence of elastin

In $Eln^{-/-}$ AA, smooth muscle cells still organize into layers surrounded by extracellular matrix (mostly collagen) in the aortic wall (Fig. 1), consistent with previous observations (Li et al., 1998; Wagenseil et al., 2009, 2010; Kim et al., 2017). Mechanically, traditional arterial strain energy functions can describe the behavior of $Eln^{-/-}$ AA, but not as well as $Eln^{+/+}$ AA (e.g. Fig. 5a), indicating that additional terms may be necessary to fully characterize the behavior in the absence of elastin. We found reduced goodness of fit for a similar strain energy function applied to the AA from mice lacking fibulin-5 ($Fbln5^{-/-}$), a critical component for assembly of elastin into mature elastic fibers (Le et al., 2015). Bellini et al. (2017) showed a higher fitting error for a similar strain energy function in 7 out of 9 different mouse models of thoracic aortic aneurysm associated with fragmented elastic fibers compared to control.

The fitted constants in the strain energy function are consistently lower in $Eln^{-/-}$ AA compared to $Eln^{+/+}$ (Fig. 5). The isotropic term is typically associated with elastin (Cheng et al., 2013; Holzapfel et al., 2000; Gasser et al., 2006), so the reduced contribution in $Eln^{-/-}$ AA is consistent with the absence of elastin in the wall. Using a similar strain

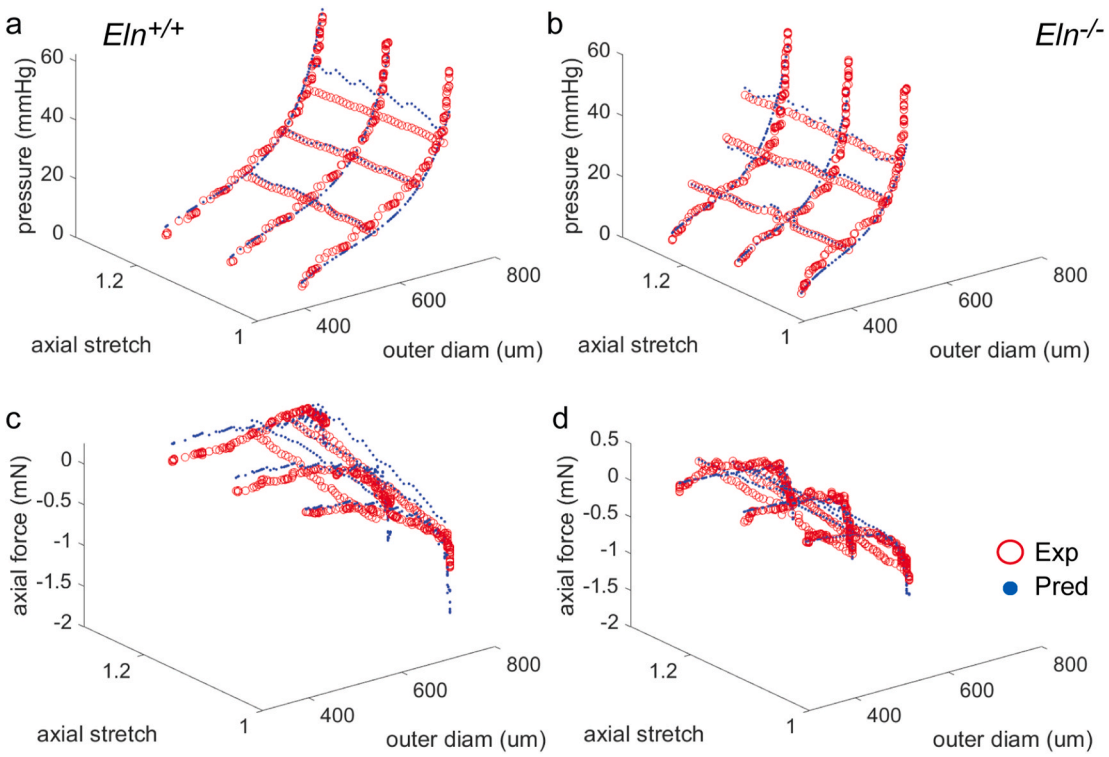

Fig. 3. Experimental and fitted data. Representative pressure (a, b) and axial force (c, d) versus outer diameter and axial stretch for $Eln^{+/+}$ (a, c) and $Eln^{-/-}$ (b, d) AA.

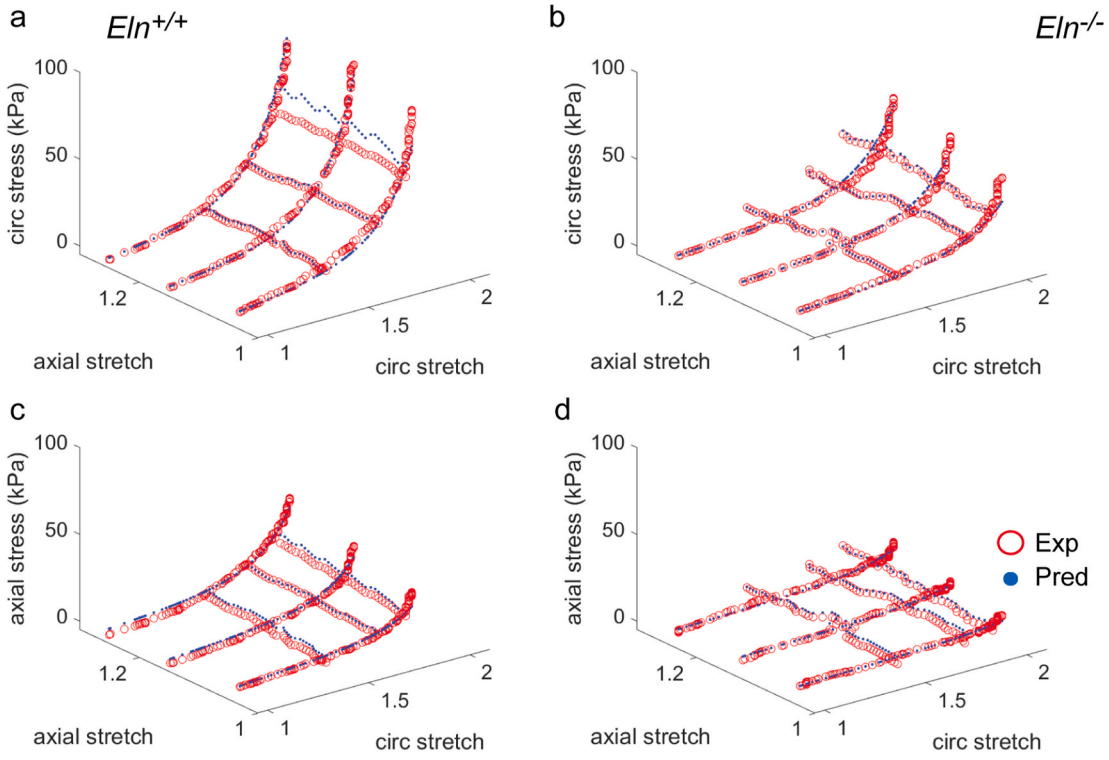

Fig. 4. Experimental and fitted stresses. Representative circumferential (a, b) and axial (c, d) stresses versus circumferential and axial stretches for $Eln^{+/+}$ (a, c) and $Eln^{-/-}$ (b, d) AA.

energy function, we found a reduced contribution of the isotropic component in heterozygous elastin ($Eln^{+/-}$) (Cheng et al., 2013) and $Fbln5^{-/-}$ AA (Le et al., 2015) compared to control at several different ages throughout postnatal maturation. Bellini et al. (2017) showed a decreased isotropic constant for a similar strain energy function in several mouse models of thoracic aortic aneurysm compared to control.

The ratio of the anisotropic constants in the strain energy function is not different between genotypes (Fig. 5f), but the absolute values are

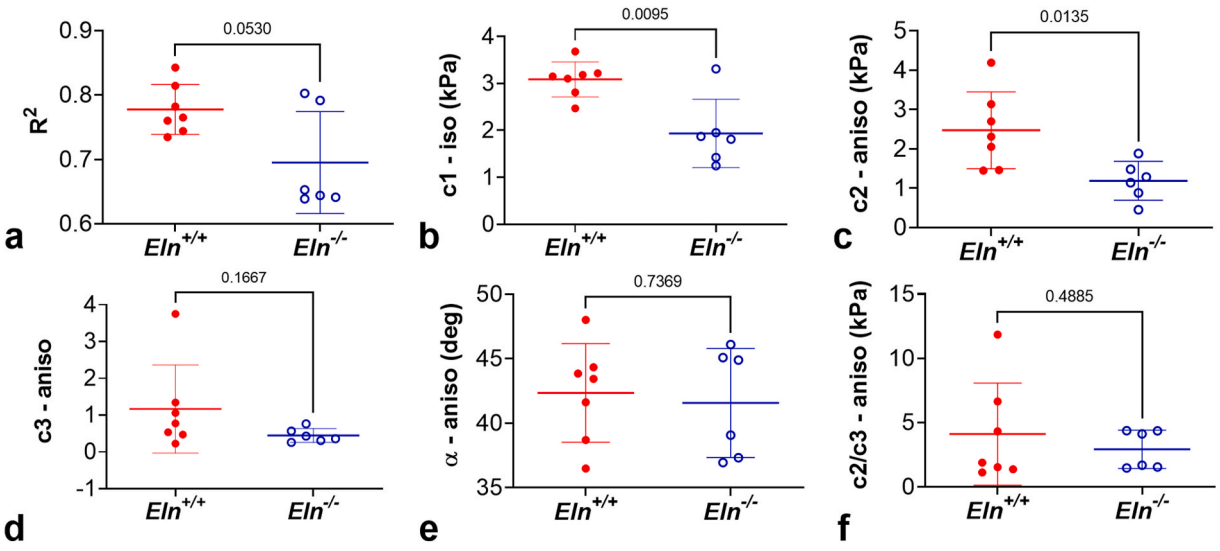

Fig. 5. Fitted strain energy constants. R^2 values (a) and fitted constants for the strain energy function for newborn $Eln^{+/+}$ and $Eln^{-/-}$ AA. Constant c_1 (b) is associated with the isotropic term and constants c_2, c_3, and α are associated with the anisotropic term as defined in Equation (8)–10. N = 6–7/group. P values from two-tailed *t*-test with Welch's correction for unequal standard deviations.

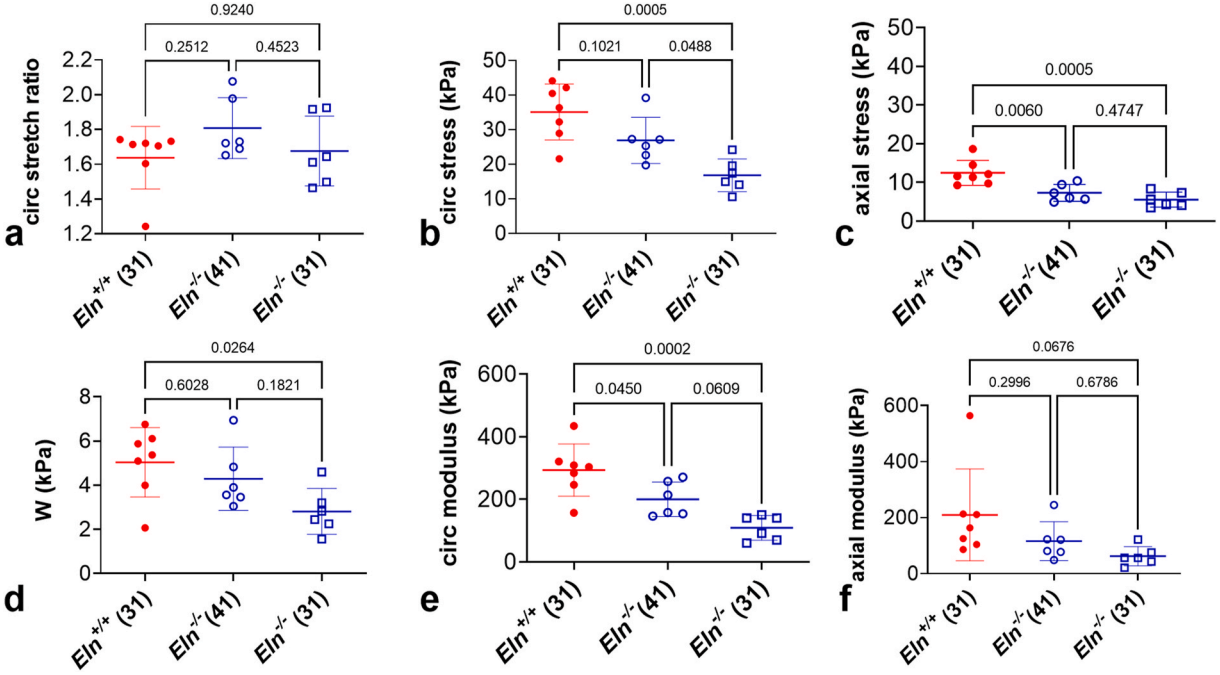

Fig. 6. Physiologic values. Stretch (a), stresses (b, c), strain energy (d), and moduli (e, f) were calculated at the physiologic pressure for each genotype. Systolic pressure is 31 mmHg in $Eln^{+/+}$ and 41 mmHg in $Eln^{-/-}$ mice (Kim et al., 2019). For comparison, the $Eln^{-/-}$ values were also calculated at 31 mmHg. N = 6–7/group. P values from one-way ANOVA followed by Tukey's multiple comparison test.

generally reduced in $Eln^{-/-}$ AA compared to $Eln^{+/+}$ (Fig. 5c and d). Since the nonlinear behavior is similar, but the absolute values of the constants are lower, the overall strain energy contribution of the anisotropic fibers is lower in $Eln^{-/-}$ compared to $Eln^{+/+}$ AA under equivalent loading conditions. The anisotropic constants are usually attributed to collagen (Cheng et al., 2013; Holzapfel et al., 2000; Gasser et al., 2006), so these results suggest that the mechanical behavior of collagen in the wall is altered by the absence of elastin. However, previous work showed that the nonlinear contribution of collagen typically increases after degradation of elastin in $Fbln5^{-/-}$ arteries (Le et al., 2015; Wan et al., 2010) or by elastase treatment (Fonck et al., 2007; Zeinali-Davarani et al., 2013) due to straightening of the collagen fibers and a decreased engagement stretch. It is possible that collagen remodeling due to the absence of elastin or elastin-related proteins in newborn aorta is different than later in maturation and adulthood or in the case of sudden elastin removal by enzymatic degradation. These differences demonstrate the importance of studying aortic remodeling at different developmental stages and from varying causes.

4.3. Changes to physiological set points in the absence of elastin

The stretch, stress, modulus, and stored strain energy of the aorta under physiologic loading conditions are important for mechanically induced remodeling and maintaining normal cardiovascular function.

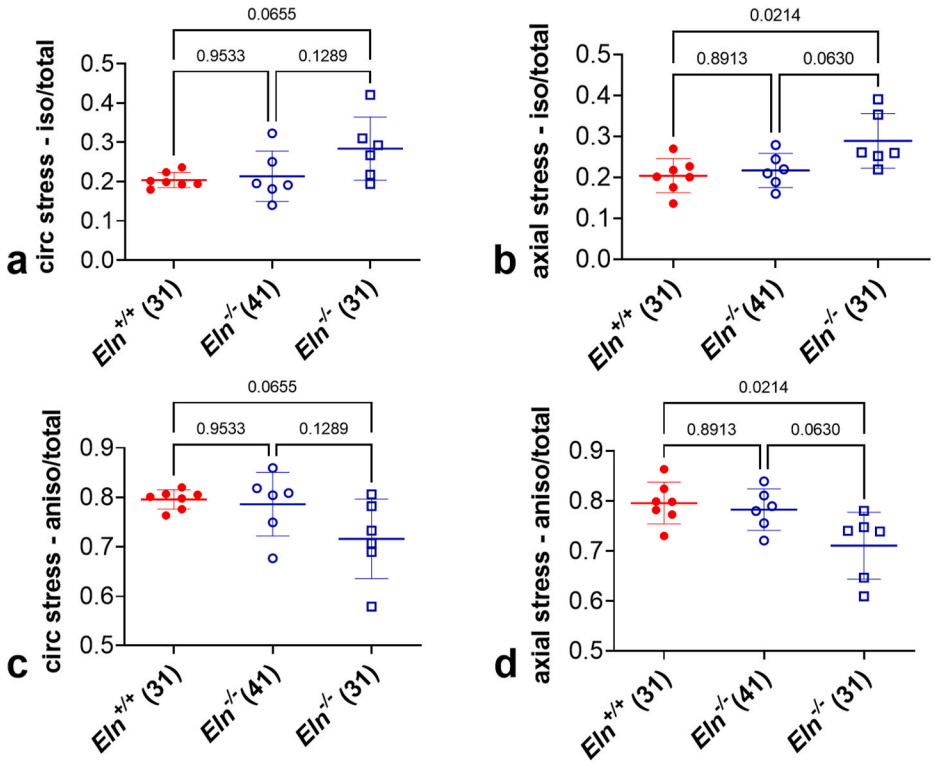

Fig. 7. Component stress ratios. The ratios of the total physiologic stresses carried by the isotropic term (a, b) and the anisotropic term (c, d) in the circumferential (a, c) and axial (b, d) directions were calculated to help understand component stress distributions in the newborn AA wall with and without elastin. N = 6–7/group. P values from one-way ANOVA followed by Tukey's multiple comparison test.

The circumferential stretch ratio is not different between genotypes (Fig. 6a). We also found that the physiologic circumferential stretch ratio is maintained within tight limits throughout postnatal maturation in *Fbln5*$^{-/-}$ and *Fbln5*$^{+/+}$ AA (Le et al., 2015), suggesting that circumferential stretch is an important parameter to control during growth and remodeling. This is consistent with the idea that smooth muscle cells in the wall are most efficient at specific stretch values due to the organization of contractile filaments (Hill, 1938). While the absolute stretch depends on the zero-stress state, which may be time dependent and may not be experienced in vivo, the contractile filament (or sarcomere) arrangement in smooth muscle cells may serve as a reference length for stretch that drives growth and remodeling (Taber, 1995).

We found that the physiologic circumferential and axial stresses and moduli are lower in *Eln*$^{-/-}$ compared to *Eln*$^{+/+}$ and that the increased blood pressure in *Eln*$^{-/-}$ mice serves to increase the values closer to those of *Eln*$^{+/+}$ mice (Fig. 6). This implies that blood pressure regulation may be a response to alterations in stress and/or moduli. We previously found that physiologic stresses and moduli are similar in young (3–20 days old) AA, but are typically higher in older (21–60 days old) AA from mice with fragmented (*Fbln5*$^{-/-}$) or reduced amounts (*Eln*$^{+/-}$) of elastic fibers (Cheng et al., 2013; Le et al., 2011, 2015) indicating continual remodeling with maturation as the hemodynamic forces increase. Smooth muscle cell contractility (Steucke et al., 2015) and differentiation (Nagayama and Nishimiya, 2020) depend on the moduli of the surrounding extracellular environment. We have suggested a "universal elastic modulus" across adult species as a target mechanical property that is best able to provide capacitance and pulse smoothing in the pulsatile circulatory system (Wagenseil and Mecham, 2009). The linearized modulus is a function of the current stress and the slope of the stress-stretch curve (Baek et al., 2007). Stress dependent growth and remodeling is commonly applied for soft tissues (Taber, 1995). Modulus dependent growth and remodeling would involve a complex interplay between stress and stretch values that is likely not trivial to implement in computational models. Note that the modulus is different than stiffness, which is a structural property that takes into account material properties and geometry. We previously showed that stiffness is increased in *Eln*$^{-/-}$ late embryonic and newborn AA (Wagenseil et al., 2009, 2010), likely due to the increased wall thickness (Fig. 2c).

The relative stress contributions of the isotropic and anisotropic strain energy terms to the total physiologic stress may provide insight into how stress is distributed across wall components. At physiologic pressures, the contribution of isotropic and anisotropic components to the circumferential and axial stresses is similar between genotypes. However, if the groups are compared at a common pressure value of 31 mmHg, the stress contribution from the isotropic term is higher and the anisotropic term is lower in *Eln*$^{-/-}$ compared to *Eln*$^{+/+}$ AA (Fig. 7). The increased blood pressure in *Eln*$^{-/-}$ mice shifts the values to be similar to those of *Eln*$^{+/+}$ mice, perhaps to redistribute the stresses onto the anisotropic wall components in the absence of elastin. As the isotropic terms are typically associated with elastin and the anisotropic terms are associated with collagen (Cheng et al., 2013; Holzapfel et al., 2000; Gasser et al., 2006), this would serve to shift stresses off of the elastin and onto the collagen.

We did not include any strain energy terms to explicitly account for the smooth muscle cells. In previous modeling efforts for the passive mechanical behavior of postnatal maturation in the aorta, smooth muscle cells were included as a discrete family of circumferentially oriented nonlinear fibers (Cheng et al., 2013). However, fitted material constants provided almost zero stress contribution for that component. Preliminary work showed similar results for the newborn AA (Supplemental Table S3) and so we did not include an additional fiber family in our chosen constitutive equation. It is likely that the passive smooth muscle cells contribute in a complex way to both the isotropic and anisotropic components considered here. Additional investigation is needed to identify smooth muscle cell contributions to passive aortic mechanics in developing mice, especially since smooth muscle cells have a larger contribution in newborn aorta compared to adult due to reduced amounts of extracellular matrix material at this stage (Murtada et al.,

2021; Wagenseil and Mecham, 2009).

4.4. Comparisons between newborn and adult aorta

The stretch, stress, modulus, and stored strain energy of the newborn aorta under physiologic loading conditions are comparable to previous studies (Murtada et al., 2021; Cheng et al., 2013; Wagenseil et al., 2009; Kim et al., 2017). While the circumferential stretch values are similar to adult AA, the stresses, moduli, and stored strain energy of the newborn AA are an order of magnitude lower than adult AA (Bellini et al., 2017). The axial stretch ratios used in this study for newborn AA are also considerably lower than those used for biaxial mechanical testing of adult AA, although they are near those used for AA after the elastic fibers have been degraded by elastase (Bellini et al., 2017). The low axial stretch ratios and the pressure-force behavior (Fig. 3c and d) may be caused by the relatively immature state of the extracellular matrix at this stage. Recent single cell RNA sequencing data show that extracellular matrix organization and synthesis pathways are the most upregulated Reactome pathways for smooth muscle and fibroblast cells in AA from 8 day old mice (Lin et al., 2021). Comparison of stresses and moduli in the aorta throughout development and evolution suggests that additional amounts and types of extracellular matrix proteins are produced to provide the necessary strength and elasticity for increasing hemodynamic loads (Wagenseil and Mecham, 2009; Wagenseil et al., 2010). Murtada et al. (2021) propose that extracellular matrix deposition after birth in the mouse aorta serves to stress-shield the smooth muscle cells. High extracellular matrix production in the early postnatal period of the mouse AA is consistent with the stress-shielding hypothesis (Wagenseil and Mecham, 2009). The passive stress carrying capacity of isolated smooth muscle cells is estimated to be 10–15 kPa (Steucke et al., 2017) or about 30% of the physiological circumferential wall stress in newborn $Eln^{+/+}$ AA (Figs. 6b) and 3% of the wall stress in adult AA (Bellini et al., 2017). Genetically modified mice, such as $Eln^{-/-}$ and others with extracellular matrix defects, allow investigation of how smooth muscle cells respond when the stress-shielding effect is altered during maturation (Staiculescu et al., 2018).

4.5. Limitations

The newborn mouse aorta is not the ideal geometry for mechanical testing of a cylindrical pressure vessel (Fig. 2). However, performing the tests in a cylindrical geometry allows biaxial data to be collected and is closer to the physiologic loading conditions than planar biaxial testing or indentation experiments. Advanced imaging and finite element models are needed in future work to determine local stresses in the unique testing geometry (Bersi et al., 2019). Due to the delicate nature of the newborn mouse AA, we were conservative in our applied axial stretches, which may limit the nonlinear behavior captured in the axial direction. We measured only passive mechanical behavior in the current study and did not include specific terms to account for smooth muscle cell contributions to the strain energy function. Additional research is needed to investigate individual contributions of the smooth muscle cells (passive and active) and extracellular matrix in newborn AA.

5. Conclusions

Passive biaxial mechanical testing and constitutive modeling of the newborn mouse aorta with and without elastin provide material properties for the maturing aorta and in the absence of a key mechanical component. The properties serve as a starting point for growth and remodeling studies of the maturing aorta and a comparison for tissue engineered arteries with varying amounts of elastin.

Funding

This study was partially funded by NIH grants HL-115560 and HL-152420 (J. Wagenseil), HL-053325 (R. Mecham), and HL-105314 (R. Mecham and J. Wagenseil).

Declaration of competing interest

The authors declare that they have no known competing financial interests or personal relationships that could have appeared to influence the work reported in this paper.

Acknowledgements

Dr. Ruth Okamoto is acknowledged for assistance in developing the preliminary finite element model in Comsol.

Appendix A. Supplementary data

Supplementary data to this article can be found online at https://doi.org/10.1016/j.jmbbm.2021.105021.

References

Amin, M., Kunkel, A.G., Le, V.P., Wagenseil, J.E., 2011. Effect of storage duration on the mechanical behavior of mouse carotid artery. J. Biomech. Eng. 133 (7), 071007.
Amin, M., Le, V.P., Wagenseil, J.E., 2012. Mechanical testing of mouse carotid arteries: from newborn to adult. JoVE : JoVE (60).
Baek, S., Gleason, R.L., Rajagopal, K.R., Humphrey, J.D., 2007. Theory of small on large: potential utility in computations of fluid-solid interactions in arteries. Comput. Methods Appl. Mech. Eng. 196 (31–32), 3070–3078.
Bellini, C., Bersi, M.R., Caulk, A.W., Ferruzzi, J., Milewicz, D.M., Ramirez, F., et al., 2017. Comparison of 10 murine models reveals a distinct biomechanical phenotype in thoracic aortic aneurysms. J. R. Soc. Interface 14 (130).
Bersi, M.R., Bellini, C., Humphrey, J.D., Avril, S., 2019. Local variations in material and structural properties characterize murine thoracic aortic aneurysm mechanics. Biomech. Model. Mechanobiol. 18 (1), 203–218.
Brinkley, K.M., 2006. The Effect of Length to Diammeter Ratio in Mechanical Testing of Arteries. Washington University, St. Louis, MO. St. Louis.
Cheng, J.K., Stoilov, I., Mecham, R.P., Wagenseil, J.E., 2013. A fiber-based constitutive model predicts changes in amount and organization of matrix proteins with development and disease in the mouse aorta. Biomech. Model. Mechanobiol. 12 (3), 497–510.
Chuong, C.J., Fung, Y.C., 1986. On residual stresses in arteries. J. Biomech. Eng. 108 (2), 189–192.
Clifford, P.S., Ella, S.R., Stupica, A.J., Nourian, Z., Li, M., Martinez-Lemus, L.A., et al., 2011. Spatial distribution and mechanical function of elastin in resistance arteries - a role in bearing longitudinal stress. Atertio Thromb. Vasc. Biol. 31 (12), 2889–2896.
Faury, G., Maher, G.M., Li, D.Y., Keating, M.T., Mecham, R.P., Boyle, W.A., 1999. Relation between outer and luminal diameter in cannulated arteries. Am. J. Physiol. 277 (5 Pt 2), H1745–H1753.
Ferruzzi, J., Bersi, M.R., Humphrey, J.D., 2013. Biomechanical phenotyping of central arteries in health and disease: advantages of and methods for murine models. Ann. Biomed. Eng. 41 (7), 1311–1330.
Fonck, E., Prod'hom, G., Roy, S., Augsburger, L., Rufenacht, D.A., Stergiopulos, N., 2007. Effect of elastin degradation on carotid wall mechanics as assessed by a constituent-based biomechanical model. Am. J. Physiol. Heart Circ. Physiol. 292 (6), H2754–H2763.
Fung, Y.C., 1993. Biomechanics : Mechanical Properties of Living Tissues, second ed. Springer-Verlag, New York, p. 568. xviii.
Gasser, T.C., Ogden, R.W., Holzapfel, G.A., 2006. Hyperelastic modelling of arterial layers with distributed collagen fibre orientations. J. R. Soc. Interface 3 (6), 15–35.
Hill, A.V., 1938. The heat of shortening and dynamic constants of muscle. Proc. Roy. Soc. Lond. B 126, 136–195.
Holzapfel, G.A., Gasser, T.C., Ogden, R.W., 2000. A new constitutive framework for arterial wall mechanics and a comparative study of material models. J. Elasticity 61 (1–3), 1–48.
Kim, J., Procknow, J.D., Yanagisawa, H., Wagenseil, J.E., 2015. Differences in genetic signaling, and not mechanical properties of the wall, are linked to ascending aortic aneurysms in fibulin-4 knockout mice. Am. J. Physiol. Heart Circ. Physiol. 309 (1), H103–H113.
Kim, J., Staiculescu, M.C., Cocciolone, A.J., Yanagisawa, H., Mecham, R.P., Wagenseil, J. E., 2017. Crosslinked elastic fibers are necessary for low energy loss in the ascending aorta. J. Biomech. 61, 199–207.
Kim, J., Cocciolone, A.J., Staiculescu, M.C., Mecham, R.P., Wagenseil, J.E., 2019. Captopril treatment during development alleviates mechanically induced aortic remodeling in newborn elastin knockout mice. Biomech. Model. Mechanobiol.
Krahn, K.N., Bouten, C.V., van Tuijl, S., van Zandvoort, M.A., Merkx, M., 2006. Fluorescently labeled collagen binding proteins allow specific visualization of collagen in tissues and live cell culture. Anal. Biochem. 350 (2), 177–185.
Le, V.P., Knutsen, R.H., Mecham, R.P., Wagenseil, J.E., 2011. Decreased aortic diameter and compliance precedes blood pressure increases in postnatal development of elastin-insufficient mice. Am. J. Physiol. Heart Circ. Physiol. 301 (1), H221–H229.

Le, V.P., Cheng, J.K., Kim, J., Staiculescu, M.C., Ficker, S.W., Sheth, S.C., et al., 2015. Mechanical factors direct mouse aortic remodelling during early maturation. J. R. Soc. Interface 12 (104), 20141350.

Li, D.Y., Brooke, B., Davis, E.C., Mecham, R.P., Sorensen, L.K., Boak, B.B., et al., 1998. Elastin is an essential determinant of arterial morphogenesis. Nature 393 (6682), 276–280.

Lin, C.J., Hunkins, B., Roth, R., Lin, C.Y., Wagenseil, J.E., Mecham, R.P., 2021. Vascular smooth muscle cell subpopulations and neointimal formation in mouse models of elastin insufficiency. Arterioscler. Thromb. Vasc. Biol. ATVBAHA120315681.

Merla, G., Brunetti-Pierri, N., Piccolo, P., Micale, L., Loviglio, M.N., 2012. Supravalvular aortic stenosis: elastin arteriopathy. Circ. Cardiovasc. Genet. 5 (6), 692–696.

Murtada, S.I., Kawamura, Y., Li, G., Schwartz, M.A., Tellides, G., Humphrey, J.D., 2021. Developmental origins of mechanical homeostasis in the aorta. Dev. Dynam. 250 (5), 629–639.

Nagayama, K., Nishimiya, K., 2020. Moderate substrate stiffness induces vascular smooth muscle cell differentiation through cellular morphological and tensional changes. Bio Med. Mater. Eng. 31 (3), 157–167.

Patel, A., Fine, B., Sandig, M., Mequanint, K., 2006. Elastin biosynthesis: the missing link in tissue-engineered blood vessels. Cardiovasc. Res. 71 (1), 40–49.

Shen, Z., Lu, Z., Chhatbar, P.Y., O'Herron, P., Kara, P., 2012. An artery-specific fluorescent dye for studying neurovascular coupling. Nat. Methods 9 (3), 273–276.

Staiculescu, M.C., Cocciolone, A., Procknow, J., Kim, J., Wagenseil, J.E., 2018. Comparative gene array analyses of severe elastic fiber defects in late embryonic and newborn mouse aorta. Physiol. Genom.

Steucke, K.E., Tracy, P.V., Hald, E.S., Hall, J.L., Alford, P.W., 2015. Vascular smooth muscle cell functional contractility depends on extracellular mechanical properties. J. Biomech. 48 (12), 3044–3051.

Steucke, K.E., Win, Z., Stemler, T.R., Walsh, E.E., Hall, J.L., Alford, P.W., 2017. Empirically determined vascular smooth muscle cell mechano-adaptation law. J. Biomech. Eng. 139 (7).

Taber, L.A., 1995. Biomechanics of growth, remodeling, and morphogenesis. Appl. Mech. Rev. 48 (8), 487–545.

Takamizawa, K., Hayashi, K., 1987. Strain energy density function and uniform strain hypothesis for arterial mechanics. J. Biomech. 20 (1), 7–17.

Wagenseil, J.E., 2011. A constrained mixture model for developing mouse aorta. Biomech. Model. Mechanobiol. 10 (5), 671–687.

Wagenseil, J.E., Mecham, R.P., 2009. Vascular extracellular matrix and arterial mechanics. Physiol. Rev. 89 (3), 957–989.

Wagenseil, J.E., Ciliberto, C.H., Knutsen, R.H., Levy, M.A., Kovacs, A., Mecham, R.P., 2009. Reduced vessel elasticity alters cardiovascular structure and function in newborn mice. Circ. Res. 104 (10), 1217–1224.

Wagenseil, J.E., Ciliberto, C.H., Knutsen, R.H., Levy, M.A., Kovacs, A., Mecham, R.P., 2010. The importance of elastin to aortic development in mice. Am. J. Physiol. Heart Circ. Physiol. 299 (2), H257–H264.

Wan, W., Yanagisawa, H., Gleason Jr., R.L., 2010. Biomechanical and microstructural properties of common carotid arteries from fibulin-5 null mice. Ann. Biomed. Eng. 38 (12), 3605–3617.

Zeinali-Davarani, S., Chow, M.J., Turcotte, R., Zhang, Y., 2013. Characterization of biaxial mechanical behavior of porcine aorta under gradual elastin degradation. Ann. Biomed. Eng. 41 (7), 1528–1538.